International Journal of Bifurcation and Chaos, Vol. 17, No. 5 (2007) 1599–1607

COMPLEXITY IN FARADAY EXPERIMENT WITH VISCOELASTIC FLUID

C. CABEZA
Instituto de Física, Facultad de Ciencias,
Universidad de la República, Uruguay
cecilia@fisica.edu.uy

M. ROSEN
Grupo de Medios Porosos, Facultad de Ingeniería,
Universidad de Buenos Aires, Argentina
mrosen@fi.uba.ar

Received November 18, 2005; Revised May 3, 2006

A systematic experimental study of the Faraday instability in viscoelastic fluid is presented. We have used a shear thinning polymer solution in which the elastic effects are predominant within our work range. We have analyzed the dependence of the threshold instability as a function of the depth in layer. Depending on the fluid layer depth and the driving frequency, harmonic or subharmonic regimes are developed. We have focused our work on the subharmonic region and temporal and spatial behaviors were analyzed. In addition, we have used the onset acceleration to estimate the rheological properties of the fluid. These predictions are supported by experimental measurements.

Keywords: Faraday instability; parametrically surface waves; pattern formation; viscoelastic fluid.

1. Introduction

The aim of this work is to introduce a new point of view in Faraday instability in complex fluids. Typical properties of the fluid are connected with the threshold instability in order to study the dynamical behavior of the fluid. The formation of standing waves on the free surface of a narrow layer of liquid when a vertical sinusoidal oscillation is applied was reported by Faraday [1831] and is one of the classical ways to create patterns of hydrodynamic origin. This subject has become a topic of particular interest since complex structures corresponding to nonlinear systems are observed [Kudrolli & Gollub, 1996; Arbell & Fineberg, 2002]. One of the most important characteristics of this system is the multiple length and time scale that can be present simultaneously. The mechanism to explain such phenomena is the nonlinear resonant interaction between the different modes, which are developed on the free surface [Wagner *et al.*, 2000]. The symmetry of the pattern depends on the viscosity and driving force (control parameter). A great variety of patterns are obtained when a viscoelastic fluid is used.

As already stated, these oscillations generate a subharmonic instability in the free surface of the fluid when the amplitude of the excitation exceeds a threshold value. However, a harmonic response can be observed [Wagner *et al.*, 1999], when very thin layers ($\lambda \approx h$) are used, because the dissipation in the bottom boundary layer becomes dominant.

Recently many experiments have been reported using a non-Newtonian fluid [Muller & Zimmerman,

1999; Lioubashevsky *et al.*, 1999]. The memory of the viscoelastic fluid introduces an additional time scale of the relaxation time. This fact leads to interesting new phenomena. If the external driving frequency is close to the elastic relaxation time of the fluid, transition between harmonic and subharmonic regimes takes place.

In this work, we describe an experimental study of Faraday waves, with a viscoelastic fluid, in which the elastic effects are predominant in our working range and the viscosity depends on shear rate (shear thinning fluid). We have worked with finite depth and this condition allows us to neglect the influence of lateral boundaries. We could show in this work that the characteristics of the pattern (wavenumber and critical acceleration) developed on the free surface, using a square and cylinder container, are equivalent.

Besides, we have investigated the dependence of the threshold instability as function of the depth of the layer and the driving frequency. Floquet theory is applied to obtain a nonlocal Mathieu equation and determine the instability onset. We have considered a two relaxation time in the Maxwell model, in order to introduce the polymer properties in Mathieu equation and investigate the validity of Maxwell model. We present in Sec. 6 of this work some pictures that describe the spatial features of the surface in order to obtain dispersion relation.

2. Basic Equations

In this section, we present the basic differential equations as well as the boundary conditions that govern the surface wave behavior in Faraday instability. The theoretical treatment is similar to Newtonian fluid, but here we need to consider the viscosity frequency dependence, through the stress of the fluid.

We consider a horizontal plate with a fluid of height h and velocity $\mathbf{v}$. It is assumed to be an incompressible fluid ($\nabla \cdot \vec{\mathbf{v}} = 0$). The vertical axis is $\mathbf{z}$, $z = 0$ corresponds to the free surface and $z = -h$ is the bottom plate position.

The temporal evolution of the velocity field $\vec{\mathbf{v}}(\vec{\mathbf{x}}, z, t)$ is governed by the Navier–Stokes equation:

$$\partial_t \mathbf{v}(\mathbf{x}, z, t) + (\mathbf{v}(\mathbf{x}, z, t) \cdot \nabla)\mathbf{v}(\mathbf{x}, z, t) = -\frac{1}{\rho}\nabla P(\mathbf{x}, z, t) + \frac{1}{\rho}\nabla \cdot T - g(t)\widehat{e}_z$$

where $\mathbf{P}$ is the pressure, ρ = density, $\mathbf{T}$ is the stress tensor and $\mathbf{g(t)}$ is the effective acceleration given by:

$$g(t) = g + a \cdot \cos(\omega \cdot t)$$

where $\mathbf{g}$ is the acceleration of gravity, $\mathbf{a}$ is the amplitude of the external acceleration and ω is the excitation frequency. Stress tensor is a complex nonlinear function of the velocity and velocity gradient, but if the linear viscoelastic theory is valid, we can write:

$$T = \int_{-\infty}^{0} G(t - t')(\nabla \mathbf{v} + (\nabla \mathbf{v})^T)dt'$$

where $G(t - t')$ is the relaxation modulus.

For a multiple-mode Maxwell fluid model, the relaxation modulus is given by:

$$G(t - t') = \sum_i \frac{\upsilon_{0i}}{\lambda_i} \exp\left(\frac{-t - t'}{\lambda_i}\right) \tag{1}$$

where λ_i are the relaxation times of the polymer.

Perturbations of the basic states obey a linear equation:

$$\partial_t v(\mathbf{x}, z, t) = -\frac{1}{\rho}\nabla p + \frac{1}{\rho}\int_{-\infty}^{0} G(t - t')\nabla^2 v(\mathbf{x}, z, t')dt'$$

Kumar showed that the nonlocal Mathieu equation obtained [Kumar, 1999] is:

$$\frac{d^2\xi}{dt^2} + 4k^2\int_{-\infty}^{0} G(t - t')\frac{d\xi}{dt'}dt' + (\omega_o^2 - ak\cos(\omega \cdot t))\xi = 0$$

where ξ denotes the vertical displacement on the free surface, ω_o^2 is the natural resonant frequency corresponding to k-mode associated to surface patterns, and it obeys the following dispersion relation [Raynal *et al.*, 1999]:

$$\omega_o^2 = \tanh(k \cdot h)\left(g \cdot k + \frac{\sigma k^3}{\rho}\right) \tag{2}$$

For subharmonic regimes, $\omega_o = \omega/2$ and for harmonic regime, $\omega_o = \omega$.

Using a classical Floquet theory, it is possible to obtain a subharmonic instability threshold. In a first approximation, we suppose a two-times Maxwell fluid, in order to consider the viscoelastic properties of the fluid. We modify the original Kumar equation, in order to analyze the threshold

dependence with the relaxation times:

$$a = \frac{2}{k}\sqrt{\left(4k^2\sum_i \frac{\upsilon_{0i}\mathrm{De}_i}{1+\mathrm{De}_i^2}\right)^2 + \left(\omega_o^2 - \frac{\omega^2}{4} + 4k^2\sum_i \frac{\upsilon_{0i}\mathrm{De}_i^2}{1+\mathrm{De}_i^2}\right)^2} \tag{3}$$

where De_i is the Deborah number, the ratio of the relaxation time scale and time scale for the process, defined as $\mathrm{De}_i = \omega\lambda/2$.

In our work, in the low range frequency, $\mathrm{De} \approx 1$, the viscoelastic effect is predominant, but at high frequency elastic behaviors are dominant ($\mathrm{De} \gg 1$).

3. Experimental Setup

3.1. *Mechanical and optical system*

The experimental set-up consists of a square acrylic container (side: 7 cm long), mounted on a Bruel and Kjaer model 4810 vibrator, which allows vertical movements with range amplitudes between 0 and 3 mm. The vibration is driven through a function generator, (Hewlett-Packard 8116A) in order to excite the system by spatially uniform acceleration in a vertical direction, $a = a_0 \sin(\omega \cdot t)$, where a_o is the control parameter and ω is the driving frequency. The acceleration amplitude of the fluid layer has been monitored continuously by a calibrated micro-accelerometer, with $0.1\,\mathrm{m/s^2}$, (Bruel and Kjaer model 4393). The signal detected by the accelerometer has been recorded, digitalized and analyzed directly in time domain. The whole system has been carefully calibrated to avoid spurious frequencies in the excitation of the fluid layer. Temporal behavior was detected using a capacitive method. This method allows making an accurate measurement of point surface displacement [Cabeza *et al.*, 2002]. We recorded and digitalized this temporal series and we made a temporal FFT at real time in order to analyze temporal response, i.e. harmonic or subharmonic regimes.

The wavelength of the resulting standing waves can be measured with an optical device, using a standard visualization technique [Bechhofer *et al.*, 1997]. A spatial Fourier Transform was used to calculate the wave number k.

The characteristic length scales in this experiment are the wavelength $\lambda = 2\pi/k$ of the surface patterns, the size of the viscous boundary layer $\delta = \sqrt{\upsilon/\omega}$ [Cerda & Tirapegui, 1992] and the capillary length $L = \sqrt{\sigma/\rho g_0} = 2.4\,\mathrm{mm}$. In our experiment we have worked with frequencies between $24\,\mathrm{Hz} \leq f \leq 120\,\mathrm{Hz}$, and the viscous boundary layer varies between $0.77\,\mathrm{mm} \geq \delta \geq 0.27\,\mathrm{mm}$.

In addition, we consider the ratio δ/h, that represent the relation between forcing and dissipative time scales [Lioubashevsky *et al.*, 1996]. The work described here was performed for $0.07 < \delta/h < 0.19$. In this range, the system presents a subharmonic bifurcation, as observed in Newtonian fluid [Edwards & Fauve, 1994].

The viscous force is characterized by the product $k\delta$, where k is the wave number associated to instability patterns developed on the surface. When $k\delta \ll 1$, viscous effects are weak, when $k\delta \approx 1$, viscous effects are strong. We have worked in the second regime, because $k\delta$ varies between 0.4 and 1.1.

3.2. *Rheological properties*

We have used a solution of 2% Polyacrylamide of 12×10^6 $\mathrm{M_w}$ (density $\rho = 997\,\mathrm{Kg/m^3}$, surface tension 0.060 N/m). Viscosity and complex modulus were measured using a Physica MCR 300 rheometer, with 2% of error. Figure 1(a) shows the viscosity as a function of the shear rate, obtained with the rheometer. We can see that the fluid behavior corresponds to shear thinning fluid, which can be fit with a Carreau model. Figure 1(b), shows G' (elastic modulus) and G'' (loss modulus) as functions of frequency. We observe that in our work range $G' > G''$, elastic effects are predominant. We have measured the relaxation time spectrum $H(\lambda)$ with the rheometer too. A maximum of spectrum corresponds to the relaxation time 1.0 sec. The minimum and the maximum value of relaxation times correspond to 0.1 sec and 10.0 sec, respectively. As we know, these results are proportional to the molecular weight [Ferry, 1970] because the polymer solution has molecular weight distribution. Therefore, the fluid that we have used presents a complex behavior: elastic response and variable viscosity.

Rheological experiment using highly monodisperse polymer systems demonstrated that a single relaxation time is insufficient to characterize accurately the many different modes of relaxation available to long flexible polymer chains [Quinzani *et al.*, 1990]. Thus, we propose a two-times relaxation

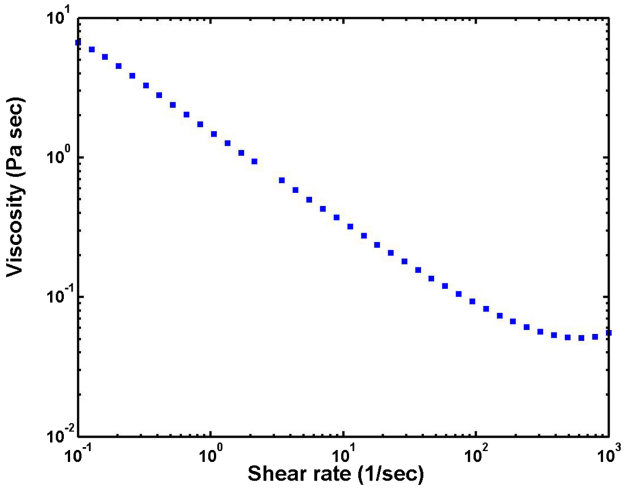

(a)

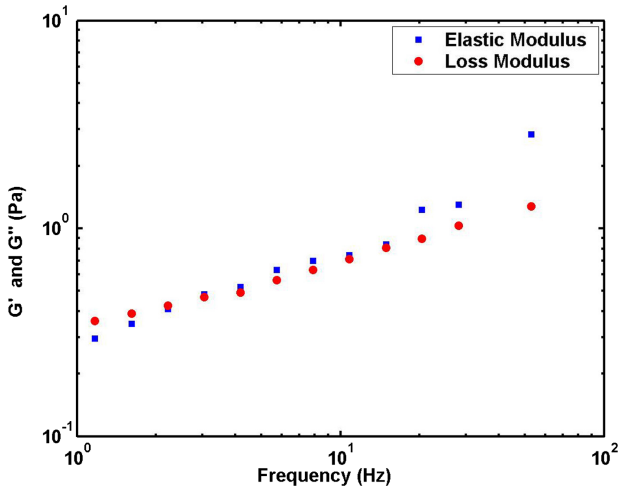

(b)

Fig. 1. Rheological properties (a) viscosity versus shear rate, (b) elastic modulus (G') and loss modulus (G'') versus frequency.

model; this is in agreement with our experimental results about the rheological properties that we have made with the rheometer.

When an oscillatory flow is applied to a viscoelastic fluid, the anisotropic stress, strain and shear rate induce global anisotropy by rearrangement of the microstructure of the fluid. The anisotropy will vary during the flow cycle in an amount determined by the size of the period of oscillation and the relaxation time.

4. Threshold Instability

For Newtonian fluid and infinite depth, linear theory predicts that the first mode that became unstable is the subharmonic mode. However, Muller *et al.* in previous works [Muller & Zimmerman, 1999] with a viscoelastic fluid and in the infinite depth limits, show that it is possible to excite an harmonic or subharmonic mode depending on the driving frequency. They found that if the driving frequency is close to the inverse of the relaxation time, an harmonic regime is developed.

In this work, we explore the influence of the depth on the dynamical behavior. In fact, the acceleration threshold depends on h, through Eq. (2). Figure 2 shows the experimental threshold amplitude a_o as a function of the driving frequency and fluid depth. We observe that for $h < 4\,\text{mm}$, the first mode that becomes unstable is harmonic for all the frequency range (24 Hz–84 Hz). Temporal behavior was detected using an experimental technique described in Sec. 3(a). Short stripes are observed on the surface. If the control parameter a_o increases, stripes evolve to hexagons, and subharmonic regime appears. For $h \geq 4\,\text{mm}$, above $f_c = 36\,\text{Hz}$, the system presents the classical subharmonic behavior, but for frequency below f_c, the harmonic mode achieves the instability threshold before the subharmonic mode. These results are in agreement with the results presented by Muller *et al.*

In order to interpret the results of this experiment, a linear analysis has been performed. Using Eq. (3), we have made a fitting between experimental and theoretical threshold accelerations.

In Fig. 3, we show the threshold amplitude acceleration as a function of the driving frequency, both theoretical and experimental. It corresponds to $h = 4.0\,\text{mm}$.

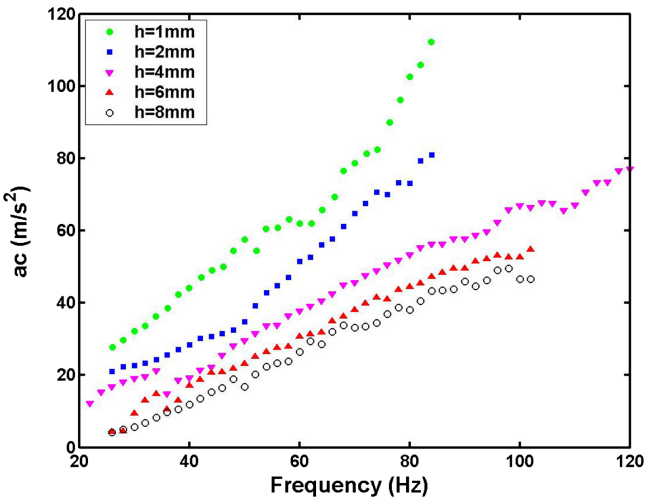

Fig. 2. Experimental results of threshold amplitude as a function of the driving frequency and fluid depth.

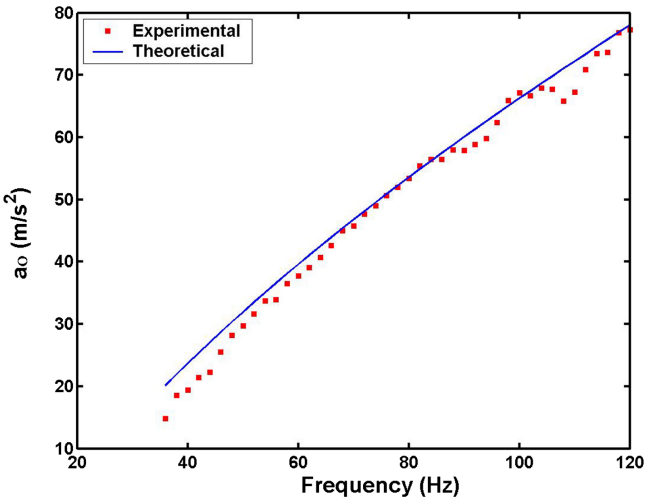

Fig. 3. Threshold amplitude acceleration for $h = 4.0\,\text{mm}$, in subharmonic regimen.

We apply Eq. (3) in order to obtain the relaxation time of the fluid. We have obtained two relaxation times values: $\lambda_1 = 6.8\,\text{sec}$, $\lambda_2 = 0.8\,\text{sec}$. The same results are obtained for $h = 4.0\,\text{mm}$ (Fig. 3), $h = 6.0\,\text{mm}$ and $h = 8.0\,\text{mm}$. These results are in the range of values obtained with the rheometer, Sec. 3.2.

5. Correlation Between Estimated Rheological Parameters and Direct Measurements

We have analyzed the correlation between experimental and estimated relaxation times with the linear relations, Eq. (3). Thus, we calculated theoretically the rheological properties of the fluid: viscosity and relaxation modulus $G(t-t')$ and we compared them with the experimental values measured with the rheometer.

Figure 4 shows an agreement between experimental and theoretical results. In conclusion, although the fluid presents high complexity, the Maxwell model of two times is a good approximation for our working range.

6. Phase Diagram of the System

An exhaustive investigation about pattern formation on the free surface of fluids for $h = 4\,\text{mm}$ has been made. In order to study the influence of boundary conditions, we used the Faraday experiment with two different geometries — cylindrical container and a square container with the same dimension characteristic length ($L_c = 70\,\text{mm}$). For

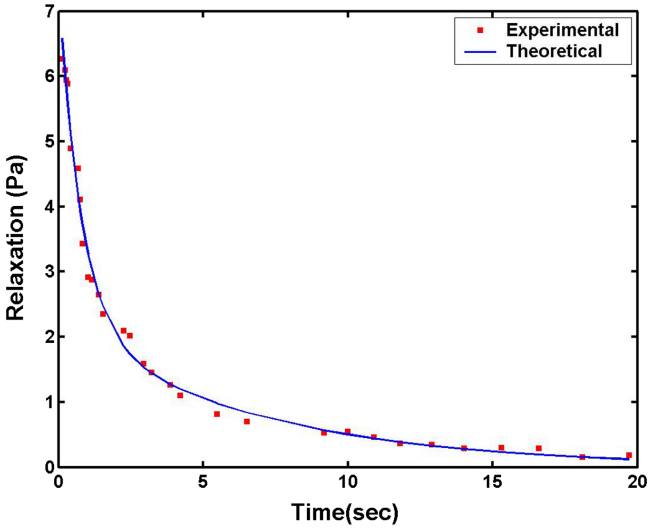

(a)

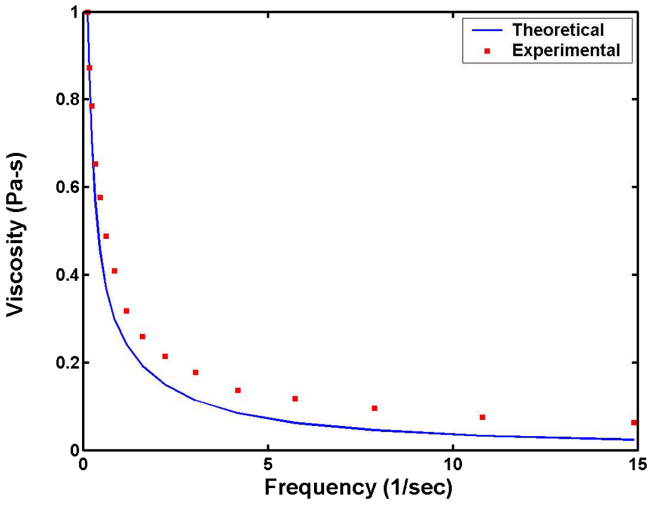

(b)

Fig. 4. Rheological properties calculated using relaxation times obtained by threshold instability. (a) Relaxation modulus versus time. (b) Viscosity versus frequency.

all images, we have calculated the wave number. It varies between 540 and 1470 m^{-1}.

Examples of the uniform primary patterns observed are shown in Fig. 5, using a square container. The patterns typically take a few minutes to equilibrate after the acceleration is increased. Patterns of different symmetry coexist in certain parameter ranges. The fact that the fluid is shear thinning (viscosity depends on frequency) allows the observation of great pattern varieties.

At low frequency, $f < 40\,\text{Hz}$, when the acceleration is increased, we can observe that hexagon-type

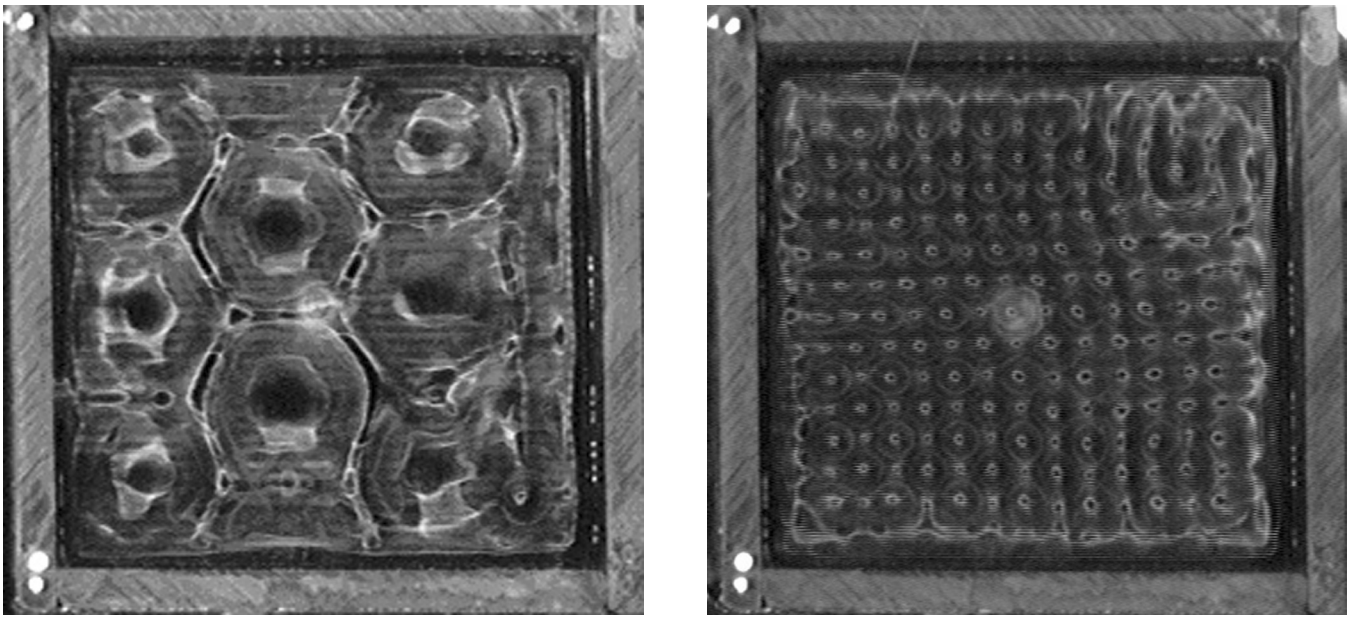

(a) (b)

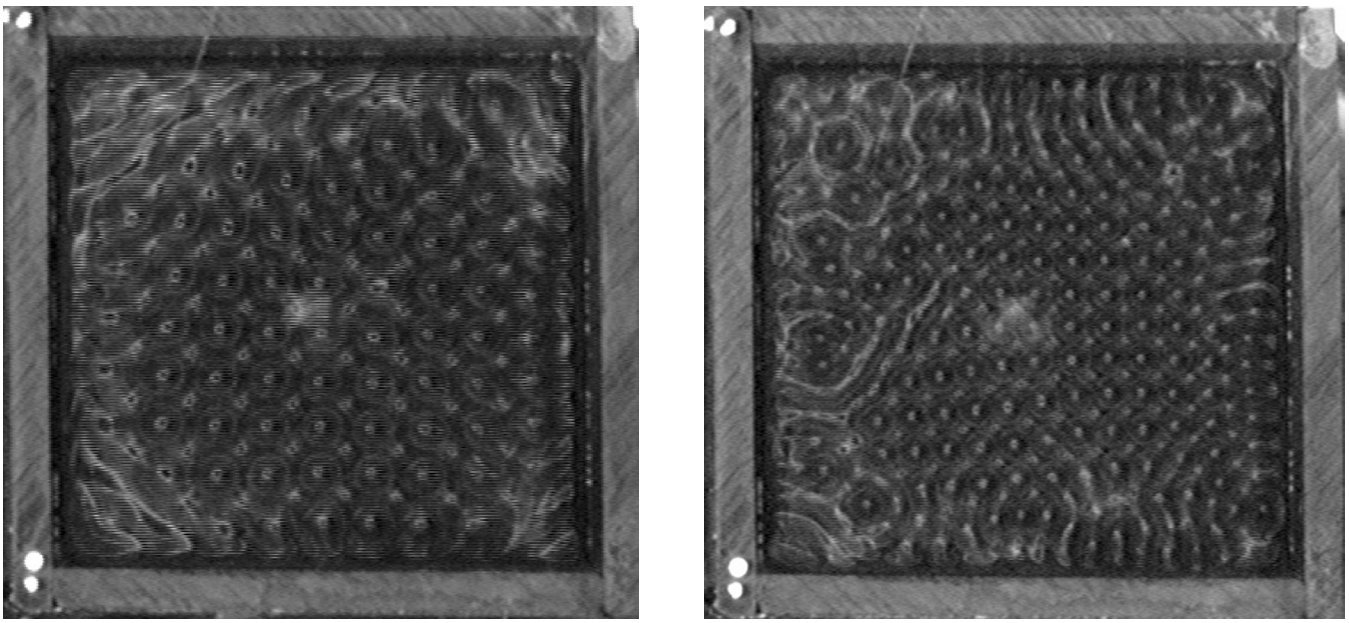

(c) (d)

Fig. 5. Patterns generated on free surface. (a) Hexagons at $f = 24\,\text{Hz}$ (b) Parallel squares at $f = 65\,\text{Hz}$. (c) Diagonal squares at $f = 50\,\text{Hz}$. (d) Coexistence of diagonal squares and hexagons at $f = 85\,\text{Hz}$.

structures are developed on the free surface. If the frequency driving is kept fixed and for higher values of acceleration, the hexagons start to become unstable and coexist with surface regions where the "crispation" behavior is present. This state is characterized by a transition to chaotic spatio-temporal behavior. There is a total break in the symmetry of the structures and a loss of coherence in the vertical movement of the points of the surface. This crispation structure spreads throughout the whole surface as this control parameter increases and just before droplet ejection.

For higher values of frequency, $f > 40\,\text{Hz}$, the dominant pattern near onset is a square pattern formed from two orthogonal standing waves, independent of the shape of the container. When we increase a control parameter (acceleration), we observe that these patterns undergo a rotation. We find that different symmetry domains often coexist. An example of this competition between squares and hexagons is shown in Fig. 5(d).

Phase diagrams in the parameter space show the patterns observed as a function of the acceleration and frequency, Fig. 6. The transition from harmonic to subharmonic regimes occurs at critical frequency, $f_c = 36\,\text{Hz}$. Zone labeled H, corresponds to hexagons patterns developed on the surface.

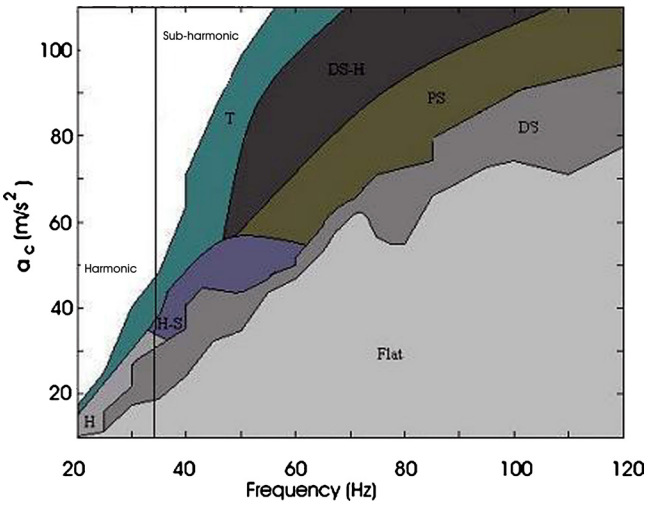

(a)

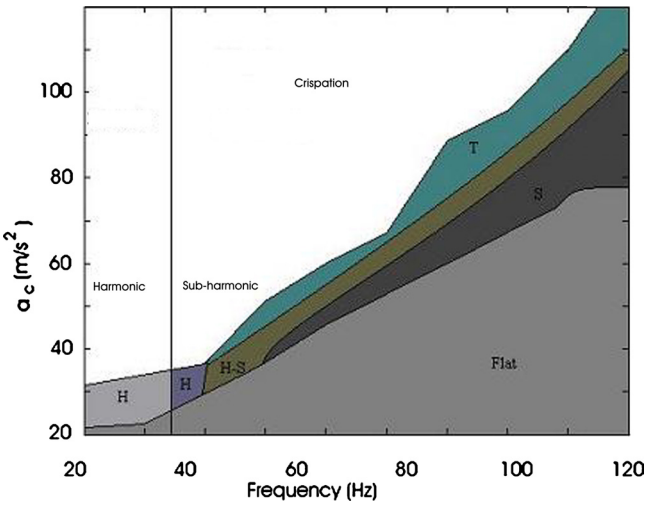

(b)

Fig. 6. Phase diagram. (a) Square container and (b) cylindrical container.

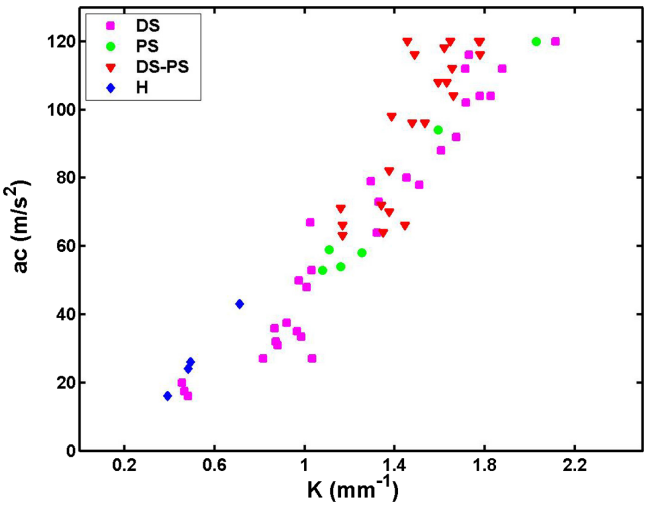

Fig. 7. Acceleration as function of wave number and pattern formation in square container. $h = 4\,\text{mm}$.

For driving frequency higher than f_c, we can observe one region where there is coexistence between hexagons and squares, labeled H–S. Zone labeled T, corresponds to transition from stable to unstable patterns. The crispation region is labeled "crispation". In the square cell, we can observe two regions labeled PS and DS, that correspond to two intermediate particular situations: at low acceleration, square structures are developed on the surface, but they present a rotation at 45° relative to the side of the cell (DS), Fig. 5(b). When control parameters increase (acceleration), squares are in alignment with the cell, denoted as PS, Fig. 5(c). For the same experimental conditions, in cylindrical containers the square orientation does not vary.

Standard techniques of FFT over the image are used in order to obtain the experimental wave number. Figure 7 shows the relationship between experimental wave number as a function of the acceleration driving, for different pattern formations on the free surface.

7. Dispersion Relation

Finally we have calculated the dispersion relationship, applying Eq. (2). It has been shown that it predicts fairly accurately the instability wavelength for Newtonian fluid [Kumar & Tuckerman, 1994]. The experimental wave number k was calculated using standard FFT over the image obtained.

Figure 8 shows the theoretical and experimental wave number as a function of the driving frequency, for $h = 4\,\text{mm}$.

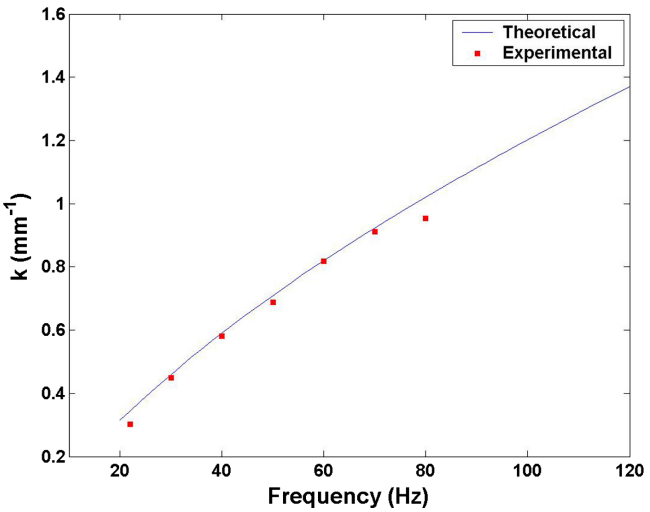

Fig. 8. Dispersion relations for $h = 4\,\text{mm}$.

We can observe a good agreement between experimental and theoretical results. In previous work, Raynal *et al.* showed that the dispersion relation for a Newtonian fluid is a good approximation to use in a viscoelastic fluid. Our experimental results are in agreement with theirs at least within the working range.

8. Conclusion

We have presented systematic experimental results on Faraday waves in a shear thinning polymer with elastic properties.

Our results confirm that the Faraday instability threshold is strongly dependent on the rheological properties of the fluid. Linear analysis of the instability acceleration threshold allows us to estimate the relaxation time of the fluid which was compared with the rheological measurement given a new contribution to the understanding of the phenomenon.

Driving frequency and layer depth are adjusted in such a way that parametrical wave on the surface with harmonic or subharmonic time dependence becomes unstable. Our results show that for $h < 4\,\text{mm}$, the system presents a harmonic temporal response. For $4 \leq h \leq 6\,\text{mm}$, we found a transition from harmonic to subharmonic regime at 36 Hz. For $h > 6\,\text{mm}$, the system presents a classical subharmonic response. The different time dependencies lead to different nonlinear patterns selection mechanism, which favors either squares or hexagons.

In addition, the influence of boundary condition is investigated. In the square cell we observed that there is larger variety of patterns selected on the free surface than in the cylindrical cell. Our experiment complemented the results obtained by other authors with another type of fluid [Wagner *et al.*, 2003].

Acknowledgments

This work has been supported by the Project URU/84/002/UNDP Uruguay, PIP 02464 (CONICET, Argentina), I041 Universidad de Buenos Aires, Argentina. CLAF 2005.

References

Arbell, H. & Fineberg, J. [2002] "Pattern formation in two-frequency forced parametric waves," *Phys. Rev. E* **65**, 756–761.

Bechhoefer, J., Ego, V., Manneville, S. & Jhonson, B. [1995] "An experimental study of the onset parametrically pumped surface waves in viscous fluids," *J. Fluid Mech.* **288**, 325–350.

Cabeza, C., Negreira, C. & Gibiat, V. [2002] "Point-localized displacement measurement of the Faraday surface on a fluid," *Measur. Sci. Technol.* **13**, 1625–1630.

Cerda, E. & Tirapegui, E. [1992] "Faraday's instability for viscous fluids," *Phys. Rev. Lett.* **78**, 859–862.

Edwards, W. S. & Fauve, S. [1994] "Patterns and quasi-patterns in Faraday experiment," *J. Fluid Mech.* **278**, 123–148.

Faraday, M., [1831] "On the forms and states of fluids on vibrating elastic surfaces," *Phil. Trans. Soc. Lond.* **52**, 319–340.

Ferry, J. [1970] *Viscoelastic Properties of Polymers* (John Wiley).

Kudrolli, A. & Gollub, J. P. [1996] "Patterns and spatiotemporal chaos in parametrically forced surface waves: A systematic survey at large aspect ratio," *Physica D* **97**, 133–154.

Kumar, K. & Tuckerman, L. [1994] "Parametric instability of the interface between two fluids," *J. Fluid Mech.* **279**, 49–68.

Kumar, S. [1999] "Parametrically driven surface waves in viscoelastic liquids," *Phys. Fluid* **11**, 1970–1981.

Lioubashevski, O., Arbell, H. & Fineberg, J. [1996] "Dissipative solitary states in driven surface waves," *Phys. Rev. Lett.* **76**, 3959–3962.

Lioubashevski, O., Hamiel, Y. Agnon, A., Reches, Z. & Fineberg, J. [1999] "Oscillons and propagating solitary waves in a vertically vibrating colloidal suspension," *Phys. Rev. Lett.* **83**, 3190–3193.

Muller, H. W. & Zimmerman, W. [1999] "Faraday instability in a linear viscoelastic fluid," *Europhys. Lett.* **45**, 169–174.

Quinzani, L. M., Mc Kinley, G. H., Brown, R. A. & Armstrong, R. C. [1990] "Modeling the rheology of polyisobutylene solutions," *J. Rheol.* **34**, 705–748.

Raynal, F., Kumar, S. & Fauve, S. [1999] "Faraday instability with a polymer solution," *Eur. Phys. J. B.* **9**, 175–178.

Wagner, C., Muller, H. W. & Knorr, K. [1999] "Faraday waves on a viscoelastic liquid," *Phys. Rev. Lett.* **83**, 308–311.

Wagner, C., Muller, H. W. & Knorr, K. [2003] "Pattern formation at the bicritical point of the Faraday instability," *Phys. Rev. E* **68**, 066204.